AN INVESTIGATION ON THE ADSORPTION OF METHYLENE BLUE FROM WATER BY MnFe$_2$O$_4$- MODIFIED DIATOMITE

Bui Van Thang[1*], Nguyen Thi Ngoc Qui[2], Tran Thi Xuan Mai[3], and Nguyen Minh Thao[4]

[1]*Academy Affairs Office, Dong Thap University, Vietnam*

[2]*Faculty of Natural Sciences Teacher Education, Dong Thap University, Vietnam*

[3]*IT and Lab Center, Dong Thap University, Vietnam*

[4]*Research Affairs Office, Dong Thap University, Vietnam*

Corresponding author: Bui Van Thang, Email: bvthang@dthu.edu.vn

Abstract

The MnFe$_2$O$_4$/diatomite was obtained by wet chemical methods. The specific structure of the material has been determined by modern physicochemical methods. The results showed that the surface of diatomite was coated by the manganese/iron oxide nanoparticles. The prepared MnFe$_2$O$_4$/diatomite material is a good adsorbent for the removal methylene blue (MB) in water. The adsorption kinetics of MB on modulation materials are consistent with the pseudo-second-order kinetics model. The adsorption isotherms well followed the Langmuir isotherm model and maximal adsorption capacity of MB can read 151.52 mg/g at 323K. The adsorption behavior of MnFe$_2$O$_4$/modified is an endothermic and spontaneous process. The results show that MnFe$_2$O$_4$/diatomite is a promising adsorbent for the efficient removal of cationic dyes from wastewater.

Keywords: *Adsorption, diatomite, dye, MnFe$_2$O$_4$/diatomite.*

KHẢO SÁT KHẢ NĂNG HẤP PHỤ XANH METHYLENE TRONG NƯỚC BẰNG VẬT LIỆU MnFe$_2$O$_4$ BIẾN TÍNH DIATOMITE

Bùi Văn Thắng[1*], Nguyễn Thị Ngọc Quí[2], Trần Thị Xuân Mai[3] và Nguyễn Minh Thảo[4]

[1]*Phòng Đào tạo, Trường Đại học Đồng Tháp, Việt Nam*
[2]*Khoa Sư phạm Khoa học tự nhiên, Trường Đại học Đồng Tháp, Việt Nam*
[3]*Trung tâm Thực hành - Thí nghiệm, Trường Đại học Đồng Tháp, Việt Nam*
[4]*Phòng Khoa học và Công nghệ, Trường Đại học Đồng Tháp, Việt Nam*
Tác giả liên hệ: Bùi Văn Thắng, Email: bvthang@dthu.edu.vn

Tóm tắt

Vật liệu MnFe$_2$O$_4$/diatomite được điều chế bằng phương pháp hóa ướt. Cấu trúc đặc trưng của vật liệu được xác định bằng các phương pháp hóa lý hiện đại. Kết quả cho thấy bề mặt của diatomite được phủ bởi các hạt nano manganese/iron oxide. Vật liệu MnFe$_2$O$_4$/diatomite là chất hấp phụ tốt để loại bỏ xanh methylene (MB) trong nước. Động học hấp phụ MB trên vật liệu điều chế phù hợp với mô hình động học biểu kiến bậc hai. Đường đẳng nhiệt hấp phụ tuân theo mô hình đẳng nhiệt Langmuir với dung lượng phụ xanh methylene cực đại là 151,52 mg/g ở 323K. Quá trình hấp phụ MB của MnFe$_2$O$_4$/diatomite là quá trình thu nhiệt và tự xảy ra. Từ các kết quả cho thấy, MnFe$_2$O$_4$/diatomite là chất hấp phụ có triển vọng để loại bỏ thuốc nhuộm cation ra khỏi nước thải một cách hiệu quả.

Từ khóa: Hấp phụ, diatomite, thuốc nhuộm, MnFe$_2$O$_4$/diatomite.

1. Introduction

Given the rapid population growth, many developed industries have confronted climate change. Therefore, the environmental pollution has been increasing, especially in the water environment. Dyes from textile industry, leather shoe production, pharmaceuticals, cosmetics is the most important agents to waste water resources (Dang et al., 2016; Sun et al., 2017). In many dye kinds, cationic dyes are more poisonous than the anionic ones. The cationic easily interact with the negatively charged cell membrane. They can also pervade and accumulate in the bio cells (Bayramoglu, G. et al., 2009). The textile dyeing wastewater has been listed as the most important pollutants because of their high toxicity and the low bio decomposition. Therefore, many scientists have been interested in treating the wastewater containing cationic dyes, to save the environment (Dai et al., 2021; Pang et al., 2019; Sun et al., 2017).

In many decades, the different methods have been developed to remove dyes in water as adsorption (Azha et al., 2019; Sun et al., 2017), the photocatalyst decomposition (Dai et al., 2021; Pang et al., 2019), flocculation (Guibal & Roussy, 2007), and bio-decomposition (Kornaros & Lyberatos, 2006). In these methods, the adsorption method is one of the most efficiency and simplest methods to treat dyes in solutions. Some different adsorbents have been used including activated carbon (Ramírez-Aparicio et al., 2021), zeolite (Supelano et al., 2020), montmorillonite (Abdul Mubarak et al., 2021), diatomite (Pang et al., 2019). However, they have not been treated after adsorption, which challenges practical application.

Recently, magnetic nanoparticles have been used in the field of adsorption and catalyst by many scientists (Dai et al., 2021; Liang et al., 2015; Pang et al., 2019). Magnetic nanoparticles can adsorb strongly and can be reproduced by magnetic methods for reusing. Many magnetic nanoparticles as manganese oxide (He et al., 2018, Islam et al., 2019), iron(III) oxide hydrate (Pan et al., 2010), and ferric oxide (Gonawala & Mehta, 2014) have been widely used for this purpose. However, magnetic nanoparticles tend to conglomerate, which decreases their surface's area and adsorption efficiency. To solve this problem, some nanosized metal oxides dispersed on different carrier substances as bentonite (Belachew & Bekele, 2020), zeolite (Li et al., 2015), and diatomite (Bui et al., 2021; Pang et al., 2019). Compared with the system of only metal oxides, the heterogeneous system is more efficient. Since the natural diatomite has high surface's area, high porosity and chemical stability, they are widely used as the carrier of catalysts, building material, material for filter and treat wastewater. The reserves of diatomite in nature are abundant. Diatomite is the fitness carrier for nanosized metal oxides through preventing the agglomeration of metal oxide particles. Therefore, these particles can contact directly with water pollutants.

In this study, the magnetic nanoparticles of $MnFe_2O_4$ are distributed on the surface of pure diatomite by the hydrothermal method and their ability in treating methylene in water is investigated. The study of adsorption kinetics, adsorption isotherms, and adsorption thermodynamics, and adsorption mechanism are done based on the experimental results.

2. Experiment and methods

2.1. Materials

In this study, diatomite from Phu Yen (RD) is used to have the purified carrier. The used chemicals are at pure analysis level of China as manganese (II) sulfate monohydrate $MnSO_4.H_2O$; iron (III) sulfate $Fe_2(SO_4)_3$; acid hydrochloric; sodium hydroxide, methylene blue (MB). The structure and general properties of MB are presented in Table 1.

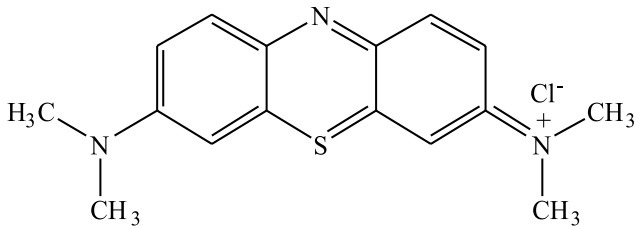### 2.2. Synthesis of $MnFe_2O_4$/diatomite material

The $MnFe_2O_4$/diatomite material have been prepared by the co-precipitation method based on the report by Pang et al. (Pang, J. et al., 2019) with some innovations: Provide 2.00 gram $Fe_2(SO_4)_3$ and 0.85 gam $MnSO_4.H_2O$ (the ratio of Fe/Mn is 2/1) into an erlen of 100 ml distilled water, heating up and stirring on the magnetic stirrer in 30 minutes at 60°C. Then, add 5.00 gram diatomite into solution and stir about 30 minutes to have a uniform system. Then, 35 ml of NaOH 1,0 M is dropped into the above erlen and stir 1.5 hours at 80°C. Finally, the brown solid is obtained by the vacuum filter and the distill water, dry at 60°C

in 12 hours. To obtain the better catalyst, the product is heated at 400ºC in 1 hour with the heating rate of 10ºC/min (the symbolized sample as $MnFe_2O_4$-D).

Besides, the $MnFe_2O_4$ material is also prepared by the equivalent method without diatomite (the symbolized sample as $MnFe_2O_4$).

Table 1. The structure and general properties of methylene blue

Name	Structure	Molecule formula	Molecule weight (g/mol)	λ (nm)
MB		$C_{16}H_{18}ClN_3S$	319.8	664

2.3. Material characterization methods

The crystal structure of diatomite and the modified diatomite is determined by X-Ray Diffraction (XRD) on D8 Advance-Bruker (Germany) with the photon 40 kV, 300 mA, angle of 1-50º. The surface area BET of samples are calculated from the nitrogen adsorption-desorption isotherm at 77K with the Micromeritics TriStar 3000 (America). The SEM images of the diatomite and modified diatomite are collected from Hitachi S-4800 (Japan). The zeta potential of these samples is determined at the different values of pH by Horiba SZ-100 (Japan), the pH value is controlled by adding NaOH or HCl solution.

2.4. Survey the MB adsorption on the $MnFe_2O_4$/diatomite

The MB solutions are prepared by dissolving MB into distilled water. The pH values of the initial solutions are controlled by the solutions of HCl 0.1 M or NaOH 0.1 M. The treatment efficiency of $MnFe_2O_4$-D is evaluated by the MB adsorption in water. Pour 0.1 gram material into 100 ml of MB solutions with the different concentrations. At the time of t minutes, about 5 ml MB solution in the treating erlen is given out and filtered. The MB samples at t minutes are analyzed by UV-Vis UV2650 (Labomed, USA) at wavelength of 664 nm. Effects of pH are surveyed in a range of 2-10. The pH values of MB solutions are changed by adding NaOH 0.1 M of HCl 0.1 M.

The capacity of MB adsorption in water by the prepared material is calculated by the formula (1):

$$q_e = \frac{C_0 - C_e}{m}.V \quad (1)$$

where C_0 (mg/L) and C_e (mg/L) is the initial concentration and equal concentration of the MB solution; m (g/L) is the weight of the used adsorbent; V is volume of the adsorption solution (L); q_e (mg/g) is the weight of the absorbed MB on 1.0 gram of RD or $MnFe_2O_4$-D material.

3. Results and discussion

3.1. Featuring $MnFe_2O_4$/diatomite material

The XRD diagram of diatomite and the modified diatomite are displayed in Figure 1. The strong intensity peak at $2\theta = 20.8º$ and $26.5º$ (Figure 1a) feature the quartz SiO_2 particles in diatomite (JCPDS No.83-2465). Some weak peaks at $2\theta = 22.0º$; $28.4º$; $31.5º$; $36.2º$ can express for the planes (101), (111), (102), and (200) of cristobalite SiO_2 (JCPDS No.76-0938) (He et al., 2018, Pang et al., 2019). The peaks of $MnFe_2O_4$ (Figure 1b) is agreed with the structure of spinel (JCPDS No.74-2403) (Pang et al., 2019). In the XRD of the $MnFe_2O_4$-D in Figure 1c, the peaks at $2\theta = 21,9º$ and $36,1º$ are the characteristic peaks of diatomite and $MnFe_2O_4$. In addition, the last peaks are not observed clearly, showing that the kinds of the amorphous oxides are mainly formed on the surface (Pang et al., 2019). The

XRD pattern (Figure 1) shows that the samples have poor crystallization, many defects, and amorphous level, likely suitable as adsorbents.
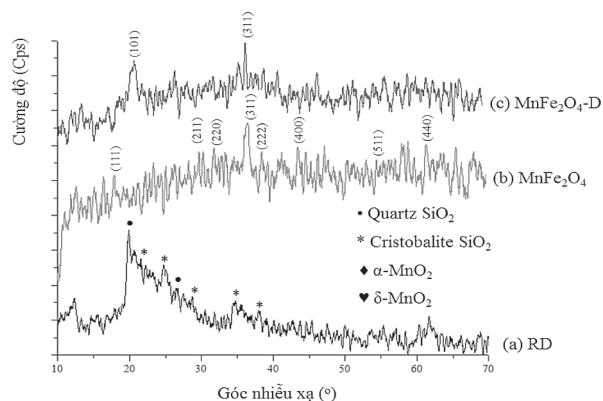

Figure 1. XRD patterns of (a) diatomite (RD), (b) $MnFe_2O_4$ and (c) $MnFe_2O_4$-D

The surface morphology of diatomite and the modified diatomite show in Figure 2. Figure 2a and 2b indicate that diatomite has high porosity with the sphere and the average porous diameter is 300-400 nm. This is the ideal hard mold material for preparing the 3D material that is widely applied. Figure 2c and 2d show that many nanoparticles with size of several ten nanometer are distributed on the surface of diatomite, thus preventing nanoparticles agglomeration. The $MnFe_2O_4$-D material has higher porosity and coarser; thus increasing surface's area can increase the ability of treating dyes.

The results of the EDX analysis of diatomite and $MnFe_2O_4$-D are shown in Figure 3. The spectroscopy of the diatomite sample contains the characteristic peak of the main elements including C, O, Al, Si, Fe, and some trace elements. In the spectroscopy of the $MnFe_2O_4$-modified RD in Figure 3, besides the above elements, there are the peaks of Mn, Fe with the higher intensity. This indicates that the diatomite has been modified successful by $MnFe_2O_4$. This result is aligned with the SEM analysis in Figure 2.
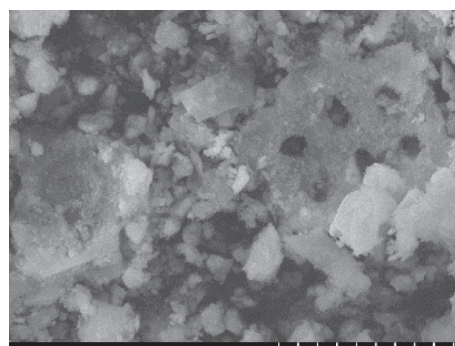
The percent of some elements of RD and $MnFe_2O_4$-D shown in Table 2 present that these elements of O, Si, Al, Fe, C are mainly in weight and some trace elements include S, Cl, Mg, Na… In the $MnFe_2O_4$-modified diatomite, the percent of Fe increases from 3.75% (RD) to 22.60% ($MnFe_2O_4$-D), and the percent of Mn is 11.06% ($MnFe_2O_4$-D). In the $MnFe_2O_4$-D, the mol ratio of Fe:Mn is 2:1, same with the ratio of the prepared precursors.
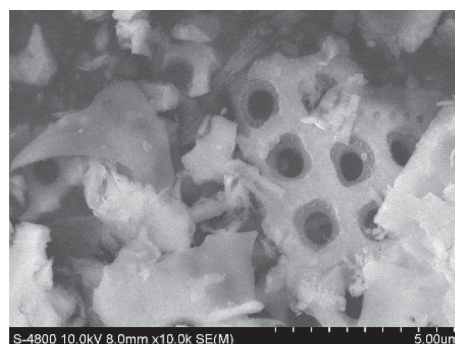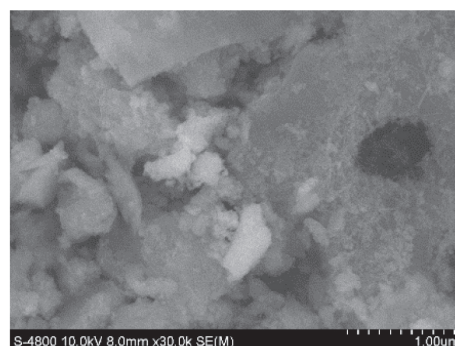

(a)
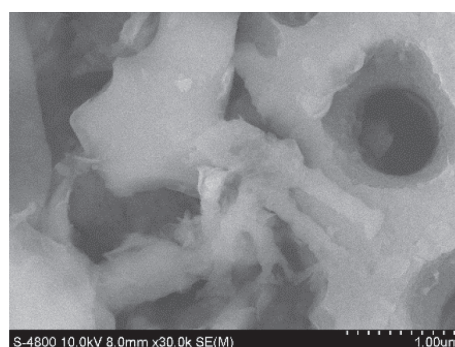
(b)

(c)

(d)

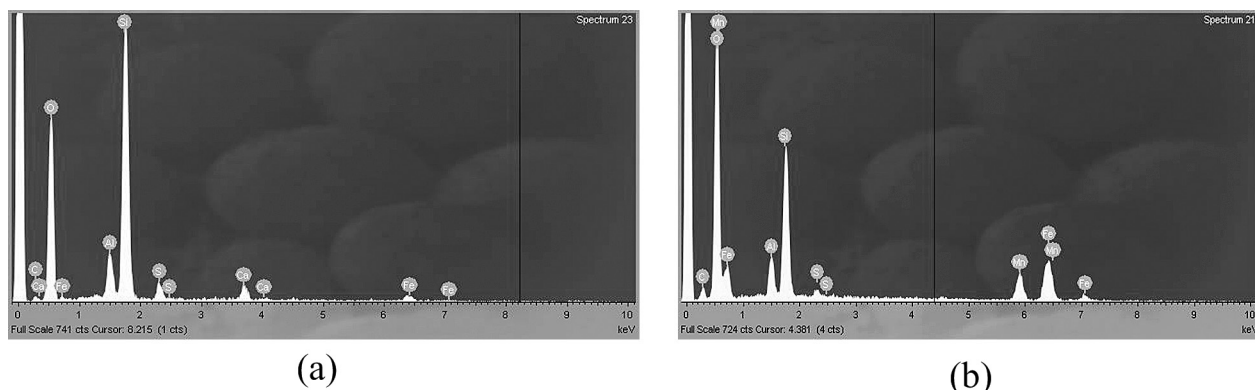**Figure 2. SEM images of RD (a, b) and $MnFe_2O_4$-D (c, d)**

(a) (b)

Figure 3. The EDX spectroscopy of RD (a) and MnFe$_2$O$_4$-D (b)

Table 2. The percent (%) of elements in RD and MnFe$_2$O$_4$-D

Elements	RD		MnFe$_2$O$_4$-D	
	% Weight	% Element	% Weight	% Element
C	3.93	6.43	4.82	9.12
O	53.49	65.77	43.69	62.42
S	2.43	1.49	0.74	0.53
Ca	3.00	1.47	-	-
Fe	3.75	1.32	22.60	9.25
Mn	-	-	11.06	4.60
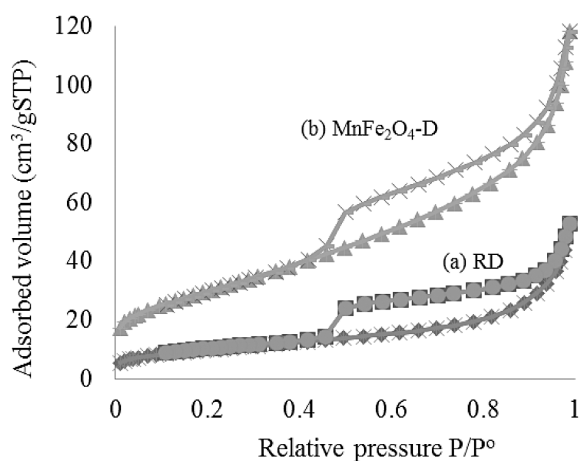
Figure 4. The N$_2$ adsorption/desorption isotherm of adsorbent (a) RD and (b) MnFe$_2$O$_4$-D

Figure 5. The distribution of porous size of adsorbents: (a) RD and (b) MnFe$_2$O$_4$-D

The nitrogen adsorption-desorption isotherm and the porous size distribution of diatomite and MnFe$_2$O$_4$-D are shown in Figure 4 and Figure 5. According to IUPAC, the adsorption-desorption isotherm of RD and MnFe$_2$O$_4$-D are the model IV. At the low pressure ($P/P_o < 0,4$), amount of adsorbed N$_2$ increases slowly with the relative pressure, the two curves of adsorption and desorption are almost identical due to monolayer adsorption (Yu et al., 2015). In addition, the weight of adsorbent increases fast at the relative pressure of $P/P_o > 0,4$. The hysteresis ring is clearly in the relative

pressure range (P/P_o) from 0.45 to 0.95, which is the characteristic of capillary condensing material. The kind of nitrogen adsorption-desorption isotherm curve and the hysteresis ring indicate that the material has a mesoporous structure with the small porous. The porous size distribution of diatomite and $MnFe_2O_4$-modified diatomite in Figure 5 show that the porous size of modified diatomite is from 3 nm to 80 nm, and the main size from 3 nm to 8 nm.

The structural parameters as the area surface BET, the porous size, the porous volume are shown in Table 3. The area surface BET of RD and $MnFe_2O_4$-D are 57.63 and 107.98 m²/g, respectively. The porous size 's distribution in BJH show that the average diameter of RD is 5.65 nm and that of $MnFe_2O_4$-D is 7.33 nm. The surface area of $MnFe_2O_4$-D is larger than diatomite, so the ability of treating the dyes increases. The surface area of $MnFe_2O_4$-D in this study is higher than the reported result in different studies as FM-diatomite: 58.1 m²/g (Son et al., 2016); FMBO-diatomite: 15.04 m²/g (Chang et al., 2009); $MnFe_2O_4$/DE: 85.03 m²/g (Sun et al., 2017).

Table 3. Some porosity parameters of RD and MnFe₂O₄-D

Samples	S_{BET} (m²/g)	S_{mic} (m²/g)	S_{ext} (m²/g)	V_P (cm³/g)	D (nm)
RD	57.63	21.66	35.97	0.0778	5.65
Diatomite (Son, 2017)	51.88	14.7	37	-	-
MnFe₂O₄-D	107.98	7.93	100.05	0.0036	7.33

S_{BET}: area surface BET;

S_{mic}: microcapillary area calculated by t - plot method;

S_{ext}: external surface area calculated by t - plot method;

V_p: capillary volume calculated from the desorption curve by BJH method;

D: average size of particle calculated from the desorption curve by BJH method.

3.2. Results of treating MB by MnFe₂O₄/diatomite

3.2.1. Adsorption kinetics

For better understanding adsorption properties of the cationic dyes, the relative between the reaction time and adsorption capacity of the MB adsorption by $MnFe_2O_4$-D, RD, and $MnFe_2O_4$ are observed, and their results are presented in Figure 6. The rate of removing MB by adsorbents increases fast and equal at 15 minutes. The fast rate indicates that the interaction between the adsorbent's surface and MB is strong. These results show that the ability of MB adsorption is higher than that of RD.

Two kinetic models are usually applied to analyze the experimental data and assess the adsorption mechanism are kinetic models of pseudo-first order (2) and pseudo-second order models as the following formulas:

$$\ln(q_e - q_t) = \ln q_e - k_1 t \quad (2)$$

$$\frac{t}{q_t} = \frac{1}{k_2 . q_e^2} + \frac{t}{q_e} \quad (3)$$

where, q_t and q_e (mg/g) are the adsorption capacity at t minutes and at the equal point; k_1 (min⁻¹), k_2 (g.mg⁻¹.min⁻¹) are the adsorption rate contanst of the kinetic models of pseudo-first order and pseudo-second models. The values of q_e and k_1 are determined from the linear line of $\ln(q_e$-$q_t)$ and t. The values of q_e and k_2 are determined from the linear line of t/q_t and t.

The linear lines of kinetic models of the MB adsorption on $MnFe_2O_4$-D are shown in Figure 7 and the parameters of kinetic models of pseudo-first order and pseudo-second models are shown in Table 4. Correlation coefficients (R^2) are both high. However, correlation coefficients of pseudo-second model is higher than pseudo-first model. Therefore, this adsorption happens by the sharing or changing electron between adsorbent and MB

(Sun et al., 2017). In addition, the maximum of MB adsorption capacity of $MnFe_2O_4$-D is 99.01 mg/g.
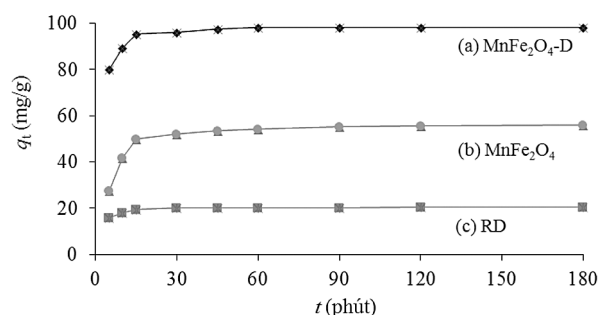
Figure 6. Effect of time to the MB adsorption capacity of material
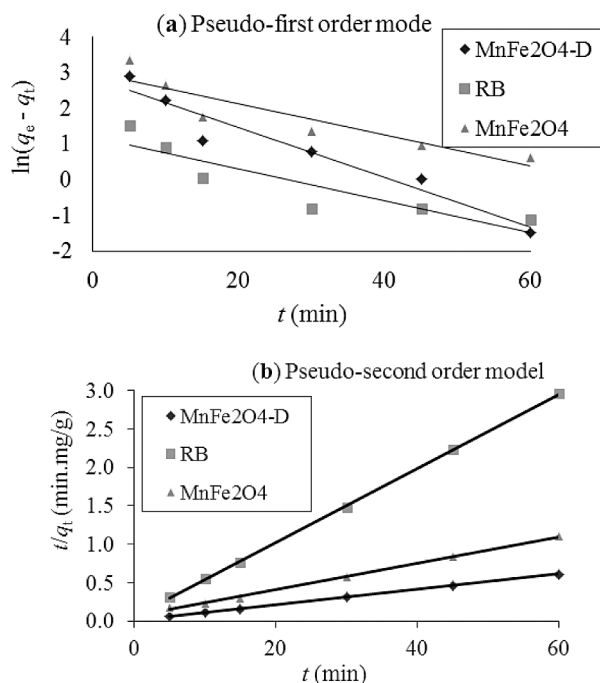
Figure 7. The linear shape of the kinetic models of the MB adsorption process by $MnFe_2O_4$-D, RD, and $MnFe_2O_4$: (a) pseudo-first order model; (b) pseudo-second order model

Table 4. Some kinetic parameters of pseudo-first order and pseudo-second order models

Adsorbent	The pseudo-first order model (2): $\ln\left(q_e - q_t\right) = \ln q_e - k_1 t$		
	k_1 (min^{-1})	q_e (mg/g)	R^2
$MnFe_2O_4$-D	0.0426	43.70	0.8920
RD	0.0800	49.43	0.9866
$MnFe_2O_4$	0.0811	11.11	0.8235

Adsorbent	The pseudo-second order model (3): $\dfrac{t}{q_t} = \dfrac{1}{k_2 \cdot q_e^2} + \dfrac{t}{q_e}$		
	k_2 (g/mg.min^{-1})	q_e (mg/g)	R^2
$MnFe_2O_4$-D	0.0112	99.01	0.9994
RD	0.0039	78.74	0.9996
$MnFe_2O_4$	0.0036	22.32	0.9995

3.2.2. The adsorption isotherm

In this study, two isotherm models are usually used as the Langmuir isotherm (4) and Freundlich isotherm models (5) to assess and to propose the mechanism of treating MB by $MnFe_2O_4$-D as two below equations:

$$\frac{C_e}{q_e} = \frac{C_e}{q_m} + \frac{1}{K_L.q_m} \qquad (4)$$

$$\ln q_e = \ln K_F + \frac{1}{n}\ln C_e \qquad (5)$$

where, q_m (mg/g) is the maximum value of adsorption capacity; K_L (L/mg) is the Langmuir constant which relates to affinity of binding center and adsorption energy; K_F (L/g) is the Freundlich constant relate to adsorption capacity; $1/n$ is the experience parameter related to the adsorption intensity, the value of $1/n < 1$ shows that the adsorption process happens easily and the new adsorption positions are formed on the adsorption surface. The values of q_m and K_L are calculated from the linear curve of C_e/q_e and C_e (Figure 8). The values of K_F and n can be deduced from intercept and slope of the linear graph of $\ln q_e$ and C_e (Figure 8).
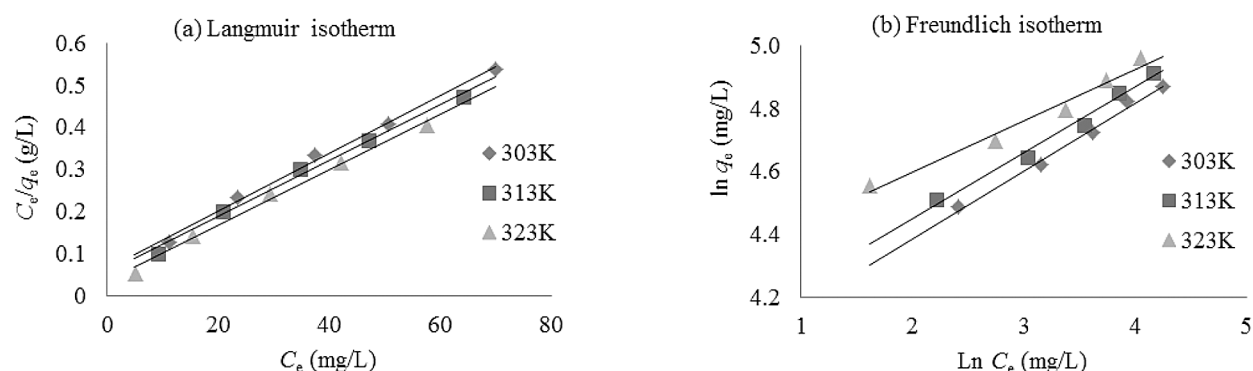
Figure 8. The linear shape of the isotherm equation the MB adsorption on MnFe$_2$O$_4$-D

Table 5. The parameters of Langmuir isotherm and Freundlich isotherm models of the MB adsorption on the modified diatomite

Temperature (K)	Langmuir (4): $\frac{C_e}{q_e} = \frac{C_e}{q_m} + \frac{1}{K_L.q_m}$		
	q_m (mg/g)	K_L (L/mg)	R^2
303	144.93	0.11	0.9956
313	149.25	0.12	0.9930
323	151.52	0.20	0.9925

Temperature (K)	Freundlich (5): $\ln q_e = \left(\frac{1}{n}\right)\ln C_e + \ln K_F$		
	$1/n$	K_F (L/g)	R^2
303	0.2162	52.09	0.9898
313	0.2090	56.32	0.9851
323	0.1636	71.51	0.9761

The isotherm study of the MB adsorption on MnFe$_2$O$_4$-D is performed at different temperatures. The results are presented in Figure 7. The ability of treating MB of material increase when the temperature increase. This indicates the adsorption process is endothermic, agreed with the before report (Sun et al., 2017). The parameters of Langmuir and Freundlich of the MD adsorption on material at different temperatures are shown in Table 5. The values of correlation coefficients of the Langmuir (R^2) are larger than that of Freundlich. So, adsorption data in Langmuir model is better than the Freundlich model in the MB adsorption on MnFe$_2$O$_4$-D. This result indicates that the MB adsorption on adsorbent is monolayer adsorption. The adsorption capacity is high at high temperature, i.e. this process is endothermic. The value of $1/n$ is less than 1 at three ranges of observed temperature, this indicates the MB adsorption on MnFe$_2$O$_4$-D is the adsorption process on the surface. In addition, the maximum capacity of MB adsorption on MnFe$_2$O$_4$-D is 151.52 mg/g (at 323K). The MB adsorption ability of some materials in some different reports are shown in Table 6. The adsorption capacity of the MB adsorption on MnFe$_2$O$_4$-D in this study is higher than different adsorbents (Sun et al., 2017). Therefore, the MnFe$_2$O$_4$-D material can remove efficiently cationic dyes in water.

Table 6. Compare the MB adsorption capacity of some adsorbents

Adsorbent	q_m (mg/g)	Reference
zeolite	55.86	(Meshko, 2001)
Fe$_3$O$_4$@APS@AA-co-CA MNPs	142.9	(Ge et al., 2012)
MnFe$_2$O$_4$/DE-NaOH	104.06	(Sun et al., 2017)
MnFe$_2$O$_4$-D	151.52	This work

3.2.3. Thermodynamics of adsorption

The parameters of thermodynamics of adsorption, standard free energy of Gibb ($\Delta G°$), standard enthalpy ($\Delta H°$), and standard entropy ($\Delta S°$) are calculated by using the following formulas (Sun, Z. et al., 2017).

$$\Delta G^o = \Delta H^o - T.\Delta S^o \quad (6)$$

$$\ln K_d = \frac{\Delta S^o}{R} - \frac{\Delta H^o}{RT} \quad (7)$$

$$K_d = \frac{q_e}{C_e} \quad (8)$$

where, $\Delta G°$ is standard free energy; R is gas constant, 8,314 (1/mol.K); T is absolute temperature (K); $\Delta H°$ is standard enthalpy (kJ/mol); $\Delta S°$ standard entropy (J/mol.K); K_d distribution coefficient; q_e the adsorption capacity at the equal state (mg/g); C_e the concentration of the cationic dye in solution at the equal state (mg/L). The value of $\Delta H°$ and $\Delta S°$ can be estimated from intercept and slope of linear equation which is built from $\ln K_d$ and với $1/T$ (Figure 9).

The adsorption thermodynamic parameters of MB are calculated and shown in Table 7. The $\Delta H°$ value of MB is position, this process is endothermic process. The $\Delta S°$ values are position, this adsorption process causes an increase in disorder at the interface between the solid and liquid phases. The $\Delta G°$ value is negative, this process happen spontaneously. On the other hand, the $\Delta G°$ values decrease when temperature increases, this indicates MB adsorption on MnFe$_2$O$_4$-D happens easily at the higher temperature. Besides that, the $\Delta G°$ values increase when the initial concentrations increase, it agrees with different reports (Sun et al., 2017); Tseng & Tseng, 2005).
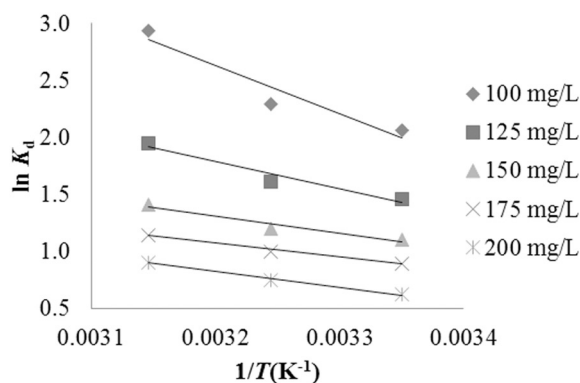
Figure 9. Plot of $\ln K_d$ versus $1/T$

3.2.4. Effect of the initial pH

Given pH of solution effects on the surface charge of adsorbent and degree of ionization of

adsorption position, the effect of pH is investigated in a range of pH 2,0-10,0. The obtained results in Figure 10 show that the adsorption ability is maximum at range of pH 4-10. To understand the adsorption mechanism, the values of zeta potential of $MnFe_2O_4$-D are determined at different values of pH. In Figure 11, the values of the zeta potential of $MnFe_2O_4$-D are negative in a range of pH 2,0-10,0. Moreover, the values of the zeta potential decrease when the values of pH increase. It plays an important role in the 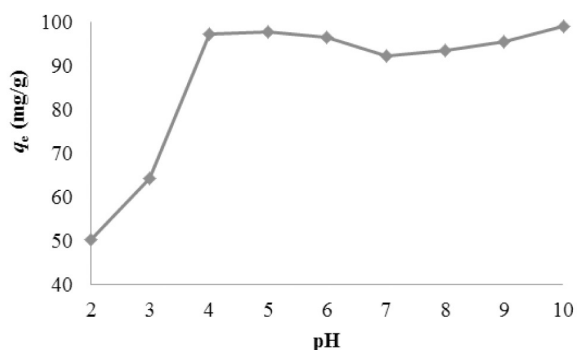adsorption process of cationic dyes due to the electrostatic attraction between the negative surface of $MnFe_2O_4$-D and cationic dyes. When value of pH decreases, the amount of positive charged position increases and the amount of negative charged position decreases. On the other hand, the negative charged position on the surface of adsorbent interacts with the cationic dyes. The adsorption is lower at acid environment because the appearance of the residual H^+ which competes with the cationic dyes at the adsorption position (Elmoubarki et al., 2015; Sun et al., 2017).
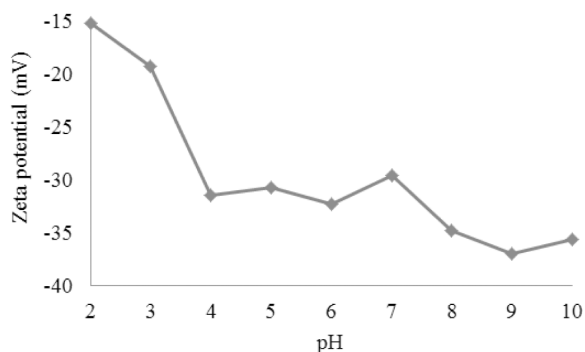

Figure 10. Effect of pH on MB adsorption by $MnFe_2O_4$-D

Figure 11. Relation between zeta potential (mV) and pH of $MnFe_2O_4$-D

Table 7. The thermodynamic parameters of MB adsorption on $MnFe_2O_4$-D at different temperatures

C_0 (mg/L)	$\Delta H°$ (kJ/mol)	$\Delta S°$ (J/mol.K)	$\Delta G°$ (kJ/mol)		
			303K	313K	323K
100	35.23	132.13	-4.80	-6.12	-7.44
125	19.96	77.73	-3.60	-4.38	-5.15
150	12.70	50.90	-2.72	-3.23	-3.74
175	10.20	41.06	-2.24	-2.65	-3.06
200	11.48	43.00	-1.55	-1.98	-2.41

4. Conclusion

The $MnFe_2O_4$/diatomite material has been prepared by hydrothermal method. The obtained material can remove the dye MB. The adsorption isotherm of $MnFe_2O_4$-D and MB can be described by the isotherm Langmuir model. The maximum of adsorption capacity is 151.52 mg/g. The adsorption capacity of $MnFe_2O_4$-D increased because the surface area is large with the porosity structure, the larger porous volume, and the more negative surface. In addition, adsorption process happens fast in the second-order kinetic model. The data of thermodynamics of adsorption indicates the nature of adsorption process is endothermic and it happens spontaneously. Therefore, the obtained $MnFe_2O_4$-D material is an adsorbent which can remove effectively cationic dyes from water./.

References

Abdul Mubarak, N. S., Bahrudin, N., Jawad, A. H., Hameed, B., & Sabar, S. (2021). Microwave enhanced synthesis of sulfonated chitosan-montmorillonite for effective removal of methylene blue. *Journal of Polymers and the Environment*, *29*(12), 4027-4039. DOI: 10.1007/s10924-021-02172-9.

Azha, S. F., Sellaoui, L., Engku Yunus, E. H., Yee, C. J., Bonilla-Petriciolet, A., Ben Lamine, A., & Ismail, S. (2019). Iron-modified composite adsorbent coating for azo dye removal and its

regeneration by photo-Fenton process: Synthesis, characterization and adsorption mechanism interpretation. *Chemical Engineering Journal*, *361*, 31-40. DOI: 10.1016/j.cej.2018.12.050.

Bayramoglu, G., Altintas, B., & Arica, M. Y. (2009). Adsorption kinetics and thermodynamic parameters of cationic dyes from aqueous solutions by using a new strong cation-exchange resin. *Chemical Engineering Journal*, *152*(2-3), 339-346. DOI: 10.1016/j.cej.2009.04.051.

Belachew, N., & Bekele, G. (2020). Synergy of magnetite intercalated bentonite for enhanced adsorption of congo red dye. *Silicon*, *12*(3), 603-612. DOI: 10.1007/s12633-019-00152-2.

Bui, V. T., Huynh, T. T. D., Tran, T. X. M., & Nguyen, M. T. (2021). An investigation on the adsorption of methyl orange from water by MnO_2-modified diatomite. *Vietnam Journal of Catalysis and Adsorption*, *10*(3), 16-25. DOI: 10.51316/jca.2021.023.

Chang, F., Qu, J., Liu, H., Liu, R., & Zhao, X. (2009). Fe-Mn binary oxide incorporated into diatomite as an adsorbent for arsenite removal: Preparation and evaluation. *Journal of Colloid and Interface Science*, *338*(2), 353-358. DOI: 10.1016/j.jcis.2009.06.049.

Dai, D., Liang, H., He, D., Potgieter, H., & Li, M. (2021). Mn-doped Fe_2O_3/diatomite granular composite as an efficient Fenton catalyst for rapid degradation of an organic dye in solution. *Journal of Sol-Gel Science and Technology*, *97*(2), 329-339. DOI: 10.1007/s10971-020-05452-3.

Dang, T.-D., Banerjee, A. N., Tran, Q.-T., & Roy, S. (2016). Fast degradation of dyes in water using manganese-oxide-coated diatomite for environmental remediation. *Journal of Physics and Chemistry of Solids*, *98*, 50-58. DOI: 10.1016/j.jpcs.2016.06.006.

Elmoubarki, R., Mahjoubi, F., Tounsadi, H., Moustadraf, J., Abdennouri, M., Zouhri, A., El Albani, A., & Barka, N. (2015). Adsorption of textile dyes on raw and decanted Moroccan clays: kinetics, equilibrium and thermodynamics. *Water resources and industry*, *9*, 16-29. DOI: 10.1016/j.wri.2014.11.001.

Ge, F., Ye, H., Li, M.-M., & Zhao, B.-X. (2012). Efficient removal of cationic dyes from aqueous solution by polymer-modified magnetic nanoparticles. *Chemical Engineering Journal*, *198*, 11-17. DOI: 10.1016/j.cej.2012.05.074.

Gonawala, K. H., & Mehta, M. J. (2014). Removal of color from different dye wastewater by using ferric oxide as an adsorbent. *International Journal of engineering Research and Applications*, *4*(5), 102-109.

Guibal, E., & Roussy, J. (2007). Coagulation and flocculation of dye-containing solutions using a biopolymer (Chitosan). *Reactive and functional polymers*, *67*(1), 33-42. DOI: 10.1016/j.reactfunctpolym.2006.08.008.

He, Y., Jiang, D. B., Jiang, D. Y., Chen, J., & Zhang, Y. X. (2018). Evaluation of MnO_2-templated iron oxide-coated diatomites for their catalytic performance in heterogeneous photo Fenton-like system. *Journal of Hazardous Materials*, *344*, 230-240. DOI: 10.1016/j.jhazmat.2017.10.018.

Islam, M. A., Ali, I., Karim, S. M. A., Hossain Firoz, M. S., Chowdhury, A.-N., Morton, D. W., & Angove, M. J. (2019). Removal of dye from polluted water using novel nano manganese oxide-based materials. *Journal of Water Process Engineering*, *32*, 100911. DOI: 10.1016/j.jwpe.2019.100911.

Kornaros, M., & Lyberatos, G. (2006). Biological treatment of wastewaters from a dye manufacturing company using a trickling filter. *Journal of Hazardous Materials*, *136*(1), 95-102. DOI: 10.1016/j.jhazmat.2005.11.018.

Li, C., Zhong, H., Wang, S., Xue, J., & Zhang, Z. (2015). Removal of basic dye (methylene blue) from aqueous solution using zeolite synthesized from electrolytic manganese residue. *Journal of Industrial and Engineering Chemistry*, *23*, 344-352. DOI: 10.1016/j.jiec.2014.08.038.

Liang, H., Zhou, S., Chen, Y., Zhou, F., & Yan, C. (2015). Diatomite coated with Fe_2O_3 as an efficient heterogeneous catalyst for degradation of organic pollutant. *Journal of the Taiwan Institute of Chemical Engineers*, *49*, 105-112. DOI: 10.1016/j.jtice.2014.11.002.

Meshko, V., Markovska, L., Mincheva, M., & Rodrigues, A. (2001). Adsorption of basic dyes on granular acivated carbon and natural zeolite. *Water research*, *35*(14), 3357-3366. DOI: 10.1016/S0043-1354(01)00056-2.

Pan, B., Qiu, H., Pan, B., Nie, G., Xiao, L., Lv, L., Zhang, W., Zhang, Q., & Zheng, S. (2010). Highly efficient removal of heavy metals by polymer-supported nanosized hydrated Fe (III) oxides: behavior and XPS study. *Water Research*, *44*(3), 815-824. DOI: 10.1016/j.watres.2009.10.027.

Pang, J., Fu, F., Li, W., Zhu, L., & Tang, B. (2019). Fe-Mn binary oxide decorated diatomite for rapid decolorization of methylene blue with H_2O_2. *Applied Surface Science*, *478*, 54-61. DOI: 10.1016/j.apsusc.2019.01.191.

Ramírez-Aparicio, J., Samaniego-Benítez, J. E., Murillo-Tovar, M. A., Benítez-Benítez, J. L., Muñoz-Sandoval, E., & García-Betancourt, M. L. (2021). Removal and surface photocatalytic degradation of methylene blue on carbon nanostructures. *Diamond and Related Materials*, *119*, 108544. DOI: 10.1016/j.diamond.2021.108544.

Son, B. H. D. (2017). *Phu Yen diatomite: modification and ít application to catalyst and adsorption. Hue University - College of Science, Vietnam.*

Son, B. H. D., Mai, V. Q., Du, D. X., Phong, N. H., Cuong, N. D., & and Khieu, D. Q. (2016). Catalytic wet peroxide oxidation of phenol solution over Fe-Mn binary oxides diatomite composite. *Journal of Porous Materials*, *24*, 601-611. DOI: 10.1007/s10934-016-0296-7.

Sun, Z., Yao, G., Liu, M., & Zheng, S. (2017). In situ synthesis of magnetic $MnFe_2O_4$/diatomite nanocomposite adsorbent and its efficient removal of cationic dyes. *Journal of the Taiwan Institute of Chemical Engineers*, *71*, 501-509. DOI: 10.1016/j.jtice.2016.12.013.

Supelano, G., Cuaspud, J. G., Moreno-Aldana, L. C., Ortiz, C., Trujillo, C., Palacio, C., Vargas, C. P., & Gómez, J. M. (2020). Synthesis of magnetic zeolites from recycled fly ash for adsorption of methylene blue. *Fuel*, *263*, 116800. DOI: 10.1016/j.fuel.2019.116800.

Tseng, R.-L., & Tseng, S.-K. (2005). Pore structure and adsorption performance of the KOH-activated carbons prepared from corncob. *Journal of Colloid and interface Science*, *287*(2), 428-437. DOI: 10.1016/j.jcis.2005.02.033.

Yu, T. T., Li, K. L., Guo, X. L., Li, F., Huang, J. M., & Zhang, Y. X. (2015). Facile decolorization of methylene blue by morphology-dependence δ-MnO_2 nanosheets -modified diatomite. *Journal of Physics and Chemistry of Solids*, *87*, 196-202. DOI: 10.1016/j.jpcs.2015.08.013.